Received: 21 February 2020 | Revised: 25 March 2020 | Accepted: 15 April 2020

DOI: 10.1002/pld3.223

ORIGINAL RESEARCH

Unoccupied aerial system enabled functional modeling of maize height reveals dynamic expression of loci

Steven L. Anderson II[1] | **Seth C. Murray**[1] | **Yuanyuan Chen**[1] | **Lonesome Malambo**[2] | **Anjin Chang**[3] | **Sorin Popescu**[2] | **Dale Cope**[4] | **Jinha Jung**[3]

[1]Department of Soil and Crop Sciences, Texas A&M University, College Station, TX, USA

[2]Department of Ecosystem Science and Management, Texas A&M University, College Station, TX, USA

[3]School of Engineering and Computer Sciences, Texas A&M University – Corpus Christi, Corpus Christi, TX, USA

[4]Department of Mechanical Engineering, Texas A&M University, College Station, TX, USA

Correspondence
Seth C. Murray, Department of Soil and Crop Sciences, Texas A&M University, 370 Olsen Blvd., 2474 TAMU, College, Station, TX 77843, USA.
Email: sethmurray@tamu.edu

Present address
Steven L. Anderson, Department of Environmental Horticulture, Institute of Food and Agricultural Sciences, Mid-Florida Research and Education Center, University of Florida, Apopka, FL, USA
Yuanyuan Chen, National Key Laboratory of Crop Genetic Improvement, Huazhong Agricultural University, Wuhan, China
Jinha Jung, Department of Civil Engineering, Purdue University, West Lafayette, IN, USA

Funding information
This project was made possible by financial support from USDA-NIFA-AFRI Award No. 2017-67013-26185, USDA-NIFA Hatch funds, Texas A&M AgriLife Research, the Texas Corn Producers Board, the Iowa Corn Promotion Board, and the Eugene Butler Endowed Chair in Biotechnology. Steven Anderson was funded for one year by the Texas A&M College of Agriculture and Life Sciences Tom Slick Senior Graduate Fellowship. Special thank you to AgReliant Genetics, LLC. and Dr. Ivan D. Barrero Farfan for conducting the genotyping for this research in kind.

Abstract

Unoccupied aerial systems (UAS) were used to phenotype growth trajectories of inbred maize populations under field conditions. Three recombinant inbred line populations were surveyed on a weekly basis collecting RGB images across two irrigation regimens (irrigated and non-irrigated/rain fed). Plant height, estimated by the 95th percentile (P95) height from UAS generated 3D point clouds, exceeded 70% correlation (*r*) to manual ground truth measurements and 51% of experimental variance was explained by genetics. The Weibull sigmoidal function accurately modeled plant growth (R^2: >99%; RMSE: <4 cm) from P95 genetic means. The mean asymptote was strongly correlated (r^2 = 0.66–0.77) with terminal plant height. Maximum absolute growth rates (mm/day) were weakly correlated with height and flowering time. The average inflection point ranged from 57 to 60 days after sowing (DAS) and was correlated with flowering time (r^2 = 0.45–0.68). Functional growth parameters (asymptote, inflection point, growth rate) alone identified 34 genetic loci, each explaining 3–15% of total genetic variation. Plant height was estimated at one-day intervals to 85 DAS, identifying 58 unique temporal quantitative trait loci (QTL) locations. Genomic hotspots on chromosomes 1 and 3 indicated chromosomal regions associated with functional growth trajectories influencing flowering time, growth rate, and terminal growth. Temporal QTL demonstrated unique dynamic expression patterns

not previously observable, and no QTL were significantly expressed throughout the entire growing season. UAS technologies improved phenotypic selection accuracy and permitted monitoring traits on a temporal scale previously infeasible using manual measurements, furthering understanding of crop development and biological trajectories.

KEYWORDS
dynamic QTL, functional modeling, maize, temporal growth, UAS, UAV

1 | INTRODUCTION

Phenotypic characterization of agricultural plant populations has lagged in scale, density, and accuracy when compared with genomic data (Pauli, Chapman, et al., 2016). Due to resource demands of labor and time-sensitive components in conventional phenotyping, most manually measured traits are acquired at only one time point in the growing season and constrained in the number of samples. This creates a limited scope of biological understanding when associating genomic information with the underlying traits of interest through plant development (Furbank & Tester, 2011). Advances in technologies including computer vision, robotics, remote sensing, and unoccupied vehicles have facilitated the development of high-throughput phenotyping (HTP) platforms which can minimize phenotypic bottlenecks (Araus & Cairns, 2014; Araus, Kefauver, Zaman-Allah, Olsen, & Cairns, 2018).

Implementation of HTP systems provides the ability to collect temporal phenotypic measurements on large representative populations within field settings, to understand how individuals interact with their environments (Araus & Cairns, 2014; Sankaran et al., 2015; Shi et al., 2016). Unoccupied aerial systems (UAS) are especially useful to increase the size of populations and field studies investigated, collecting RGB images, and reconstructing three dimensional representations of field crop trials using structure from motion methodology (Bendig et al., 2014; Holman et al., 2016; Shi et al., 2016; Chang, Jung, Maeda, & Landivar, 2017; De Souza, Lamparelli, Rocha, & Magalhães, 2017; Watanabe et al., 2017; Chu, Starek, Brewer, Murray, & Pruter, 2018; Malambo et al., 2018; Pugh et al., 2018; Anderson, Murray, Malambo, et al., 2019). UAS height estimates of maize have previously been validated using correlations to traditional manual measurements and evidence of equivalent or greater phenotypic variation partitioned to genetic factors (Anthony et al., 2014; Chu et al., 2018; Pugh et al., 2018; Anderson, Murray, Malambo, et al., 2019). To our knowledge, the majority of reported field-based phenotyping of maize with HTP platforms has focused on hybrid trials (Geipel, Link, & Claupein, 2014; Li et al., 2016; Shi et al., 2016; Varela et al., 2017; Chu et al., 2018; Malambo et al., 2018; Pugh et al., 2018; Anderson, Murray, Chen, et al., 2019; Anderson, Murray, Malambo, et al., 2019), but limited reports have been published on the evaluation of inbred trials (Han et al., 2018, 2019; Wang et al., 2019), specifically genetic mapping populations. Inbred lines in maize are substantially shorter and have less biomass than hybrids, lacking heterosis.

Maize height is important as a physiological and a highly heritable agronomic trait (Peiffer et al., 2014; Wallace et al., 2016; Anderson, Mahan, Murray, & Klein, 2018; Mahan, Murray, & Klein, 2018; Anderson, Murray, Malambo, et al., 2019) commonly collected due to its ease of measurement, agronomic importance, and correlation to hybrid grain yield in some environment and management scenarios (Mallarino, Oyarzabal, & Hinz, 1999; Machado et al., 2002; Katsvairo, Cox, & Van Es, 2003; Yin, McClure, Jaja, Tyler, & Hayes, 2011; Farfan, Murray, Labar, & Pietsch, 2013; Chen, 2016; Anderson, Murray, Malambo, et al., 2019). Manually measured plant height is commonly collected after reproductive maturity as the distance from the ground to the tip of the tassel, flag leaf, or peduncle. The genetic architecture of plant height in maize has been determined to fit an infinitesimal model (i.e., very large numbers of small additive effect loci) with some large effect loci likely fixed during domestication and early selection (Peiffer et al., 2014). Functional genetic variation in terminal plant height has been shown to be controlled through hormones: mutations within the (a) gibberellin biosynthesis pathways (Lawit, Wych, Xu, Kundu, & Tomes, 2010) and crosstalk with other phytohormones including (b) auxin (Multani et al., 2003) and (c) brassinosteroids (Winkler & Helentjaris, 1995; Hartwig et al., 2011; Makarevitch, Thompson, Muehlbauer, & Springer, 2012; Wang, Zhao, Lu, & Deng, 2017). Hormones are well known to fluctuate throughout plant growth, responding to environmental and developmental stimuli (Ferreira & Kieber, 2005; Lorenzo & Solano, 2005; Finkelstein, 2006; Huq, 2006). Traditional QTL studies using phenotypic data at a single terminal (end of season) time point can only represent accumulated effects, ignoring the dynamic nature of many agronomically important traits which, like hormones, change and can be identified as functions of time (Wu & Lin, 2006).

Growing evidence demonstrates quantitative trait loci (QTL) can be deterministic QTL (dQTL) represented as the differential allelic variation which affects the whole growth process, unaffected by environmental stimuli or opportunistic (oQTL) responding to biotic/abiotic stimuli (Wu, Wang, Zhao, & Cheverud, 2004). Function mapping has identified QTL associated with dynamic traits (a) within narrow time periods, (b) throughout the lifecycle, and (c) at specific physiological growth stages (Bac-Molenaar, Vreugdenhil, Granier, & Keurentjes, 2015; Campbell et al., 2017; Feldman et al., 2017; Ward et al., 2019). Patterns of temporal QTL associations using field-based HTP systems have been demonstrated for soybean canopy cover

(Xavier, Hall, Hearst, Cherkauer, & Rainey, 2017), cotton stress-response traits (Pauli, Andrade-Sanchez, et al., 2016), spring barley biomass accumulation (Neumann et al., 2017), wheat plant height (Lyra et al., 2020), rice yield components (Tanger et al., 2017), and triticale plant height (Würschum et al., 2014). Temporal patterns of QTL have been evaluated in maize within greenhouse setting using automated phenotyping platforms (Muraya et al., 2017; Zhang et al., 2017); to our knowledge, Wang et al. (2019) is the only reported field-based temporal QTL study in maize using HTP approaches.

Plant height is an ideal phenotype to explore the temporal patterns of QTL expression in maize. Using UAS, we evaluated three recombinant inbred line (RIL) linkage mapping populations under field conditions and captured the dynamic growth patterns of plant height across these maize inbreds. The objectives of this study were to: (a) evaluate UAS procedures developed for hybrids to estimate heights within inbred maize populations; (b) model and compare growth patterns across genetic populations; (c) evaluate temporal patterns of QTL expression through the growing season; and (d) evaluate the temporal expression patterns for previously reported QTL.

2 | MATERIALS AND METHODS

2.1 | Germplasm material and experimental design

Three bi-parental mapping populations were developed from breeding lines segregating for loci discovered in an earlier genome-wide association study (Farfan et al., 2015; Chen, 2016) of hybrids for height and grain yield. The recombinant inbred line (RIL) progeny were derived from the crosses of Tx740xNC356 (tropical/tropical; 102 RILs), Ki3xNC356 (tropical/tropical; 237 RILs), and LH82xLAMA-YC (temperate/tropical; 178 RILs). Tx740 (LAMA2002-12-1-B-B-B) (Mayfield et al., 2012) is a parent in the "LAMA" inbred line (pedigree [((LAMA2002-12-1-B-B-B-B/LAMA2002-1-5-B-B-B-B)-3-2-B-1-B3-B]), and these two lines would be expected to share 50% of their genome. In 2018, the mapping populations were planted in a randomized complete block design (RCBD) within each of two environments (irrigated and non-irrigated) with two replications per environment (i.e., 2 blocks per environment). Spatial planting dimensions were 0.76 m row spacing and 3.81 m plot lengths. The range by row spatial organization within each irrigation regimen consisted of 32-by-8, 32-by-17, and 32-by-13 ranges by rows for Tx740xNC356, Ki3xNC356, and LH82xLAMA-YC populations, respectively.

2.2 | Unoccupied aerial system image collection

Two platforms were used, a rotary wing and a fixed wing UAV, to collect RGB data. For the rotary wing, a DJI Phantom 3 Professional with a 12-megapixel DJI FC300X camera, was flown at an altitude of 25 m with 80% forward and side image overlap. Fixed wing images were collected using a Tuffwing UAV Mapper (http://www.tuffwing.com) equipped with a 24-megapixel Sony a6000 RGB camera. Fixed wing surveys were conducted at an altitude of 120 m with 80% image overlap. A total of 19 DJI Phantom 3 Professional flights were conducted throughout the growing season, while 11 Tuffwing UAV Mapper flights (starting 05/17/2018) were conducted after early season mechanical setbacks of the Tuffwing (Table S2). After QC/QA, a total of 16 flights were used for height estimates based on quality of the processed orthomosaic images.

All of the Tuffwing flights were processed in Agisoft PhotoScan (AgiSoft PhotoScan Professional, 2016), while the majority of the DJI Phantom flights were processed in Pix4Dmapper (Pix4Dmapper, 2018), based on collaborators comfort and preference with the associated software. In general, these software packages are equivalent and used to identify common features (tie points) across images followed by triangulation and distortion adjustment optimization to generate densified 3D point clouds, DSM, and orthomosaic images. Height estimates were extracted from the three-dimensional point clouds following the procedures of Anderson, Murray, Malambo, et al., 2019. In short, the ground points were identified from the point cloud using the hierarchical robust interpolation algorithm within FUSION/LDV. Identified ground points were used to interpolate the digital elevation model, followed by subtracting the digital elevation model (DEM) from the original point cloud to produce the canopy surface model. The plot-level polygon shapefiles were created using the R/UAStools::plotshpcreate (Anderson, Murray, Malambo, et al., 2019) function in R, and the 95th percentile height estimates were extracted for each experimental plot.

2.3 | Statistical inference

2.3.1 | Variance component estimates and heritability

From the extracted canopy height metrics (P95), we fit mixed linear models utilizing residual maximum likelihood (REML) in JMP version 14.0.0 (JMP®, 2018) to define best linear unbiased predictors (BLUPs) of the inbreds by their entry number. Models were fit on a per flight date basis. The individual mapping populations were evaluated as randomized complete block designs (RCBD, Equation 1) within each environment including spatial regression (range and row [furrow irrigation runs down rows], this has also been called row and column, respectively, where furrow irrigation is not used) for each of the irrigation treatments (irrigated and non-irrigated) independently.

$$Y_{ijkl} = \mu + G_i + \text{Rep}_j + \text{Range}_k + \text{Row}_l + \varepsilon_{ijkl} \quad (1)$$

With grand mean (μ) and random terms genotype ($G_i \sim N(O,\sigma^2_G)$), replicate ($\text{Rep}_j \sim N(O,\sigma^2_{\text{Rep}})$), range ($\text{Range}_k \sim N(O,\sigma^2_{\text{Range}})$), row ($\text{Row}_l \sim N(O,\sigma^2_{\text{Row}})$), and residual error ($\varepsilon_{ijkl} \sim N(0,\sigma^2)$), Fisher's least significant difference (LSD) test was performed to test for significant differences ($\alpha = 0.05$) between group means.

Broad sense heritability (H^2) estimates were calculated on an entry means basis (Equation 2).

$$H^2 = \frac{\sigma_G^2}{\sigma_G^2 + \sigma_\varepsilon^2/\text{rep}} \quad (2)$$

Within each environment, H^2 estimates were calculated for each population separately while including replicates (*r*) for each of the UAS flight dates.

2.3.2 | Nonlinear function

The three-parameter Weibull sigmoid growth model (Equation 3) was used to summarize the

$$f(x) = L\left(1 - e^{\left(-(x/x_0)^b\right)}\right) \quad (3)$$

height as a function of DAS (*x*) with the asymptote (*L*), inflection point (x_0), and the growth rate (*b*) of the fitted curve. The asymptote (*L*; m) is maximum value of the curve which represents maximum/terminal plant height (PHT_{TRML}). The inflection point (x_0; DAS) indicates the DAS where the slope of the logarithmic phase is at its absolute maximum. The growth rate (*b*) is a unitless empirical constant which defines the shape of the curve. The Weibull function differs from the classical logistic function in its assumption of the inflection point location. Logistic assumes the curve is symmetric and inflection lies halfway between zero and the asymptote, whereas Weibull inflection is more flexible to asymmetric growth and the inflection point can lie at any *x*-value (Archontoulis & Miguez, 2015).

The absolute growth rate (AGR; m/d) can be derived from the derivative of the Weibull function (Equation 4) at any *x*-value using the fitted Weibull parameters. The maximum AGR is

$$f'(x) = \frac{\text{Lbe}^{\left(-(x/x_0)^b\right)}\left(\frac{x}{x_0}\right)^b}{x} \quad (4)$$

equivalent to $x = x_0$. Sigmoidal curves were fit using the Fit Curve tool in JMP 14, and parameters were estimated on an entry basis utilizing the extracted BLUPs or the individual environment REML models described above. Significance of the functional parameters was evaluated using the chi-squared (X^2) test (α = 0.05, *df* = 1) to identify logistical curves with poor fits to UAS height estimates, and these were subsequently removed from future analysis. Using the associated Weibull functional parameters, height estimates were imputed on one-day intervals (1 to 85 DAS) for each inbred entry in their associated environments.

2.4 | Genotyping and linkage map construction

The genotyping was described in Chen (2016) and is paraphrased here. Genotype samples were collected from $F_{3:4}$ seedlings grown under greenhouse conditions, where eight samples were bulked per genotype. The CTAB method (Chen & Ronald, 1999) was used to extract DNA and samples were sent to AgReliant Genetics LLC, where they were genotyped by Infinium® assays for 17,444 single nucleotide polymorphisms (SNPs). The linkage groups and physical locations were provided with the SNP chip of which 716 marker locations were unknown or withheld due to intellectual property rights, resulting in 17,019 SNPs with known reference locations (B73 RefGEN_v3).

Individuals with >10% missing values and SNPs with >10% missing values were dropped from the data set resulting in 5,316, 5,628, and 6,231 polymorphic SNPs for the Ki3/NC356, Tx740/NC356, and LH82/LAMA populations, respectively. Crossover points were predicted to clean data set of double recombinants using the crosspoint command of SNPbinner version 0.1.1 (Gonda et al., 2018) with emission probability (*-p*) set to 0.9, continuous genotype region (*-r*) set to 0.1% of the chromosome size, and transition probability (*-c*) was calculated using a crosscount of 7,500,000. The visualize subcommand was used to evaluate the efficiency of the calculated break points to the original SNP calls and identify satisfactory crosspoint parameters. The crosspoint output identified break point locations for each RIL and the prediction of genotypic homogeneity of each region between breakpoint and the SNP calls were adjusted accordingly. Marker data sets filtered by SNPbinner were constructed into linkage maps using the MAP function of QTL IciMapping version 4.1.0.0 (http://www.isbreeding.net/) software. Redundant markers were identified using the "BIN" functionality, and redundant markers with greater missing data rate were excluded. Linkage groups were defined by "By Anchor Only" setting, and the marker orders were defined by their physical locations using the "By Input" ordering algorithm. Recombination frequencies between markers were calculated based on F_3 marker frequencies by denoting the "POP.ID" to eight.

The final genetic maps consisted of 1,530, 2,571, and 2,324 SNPs after removal of redundant markers. The genetic map distances were calculated in QTL IcIMappering using the Kosambi mapping function, and the total map lengths were estimated to be 1,315, 1,207, and 1,474 cM for the Tx740xNC356, Ki3xNC356, and LH82xLAMA populations, respectively.

2.5 | Linkage mapping

The entries phenotyped in 2018 were advanced several generations following initial DNA extraction at $F_{3:4}$ and were evaluated in the field at F_6 generation or greater. For this reason, heterozygous calls (1) were set to missing (−1) and QTL analysis was performed assuming RIL genotype frequencies ("POP.ID" = 4). Analysis by other methods (e.g., treating as F_3) were also tested to ensure conclusions were similar, but detection power was much lower, likely due to the software trying to fit dominance effects expected to be rare or absent by the F_6 generation. Inclusive composite interval mapping (Li, Ye, & Wang, 2007) of additive (ICIM-ADD) QTL were conducted in the QTL IciMapping v4.1 using the BIP (QTL mapping for bi-parental populations) function. The step parameter

was set to 1.0 cM, and the probability of inclusion in the stepwise regression (PIN) was set to 0.001. The focus of this study was on understanding the temporal shifts in the marker trait associations of plant height, rather than identifying regions of high confidence that could be used in later marker assisted selection. For these reasons, we defined QTL of interest liberally as those with LOD > 2.0 and percent variation explained ≥ 3% [66]; however, LOD and other metrics are provided to extract more conservative thresholds. Using the imputed heights from 1 to 85 DAS, ICIM-ADD was performed on each DAS, for each population in each environment separately to access the temporal shifts in allelic effects and marker–trait associations.

A list of candidate genes was obtained from Wallace et al. (2016). In short, candidate genes were identified from (a) literature, (b) mining the MaizeGDB database for known height mutants, and (c) searching the maize genome annotation on Phytozome genes annotated with "auxin," "brassinosteroid," and/or "gibberellin." Distance for the center of the QTL confidence interval to nearest candidate gene with the same chromosome was identified.

3 | RESULTS AND DISCUSSION

3.1 | UAS surveys and image processing quality

A total of 18 and 11 flights were conducted over the bi-parental mapping populations using the DJI Phantom 3 Pro and Tuffwing UAV Mapper, respectively (Table S1). Early season DJI Phantom 3 Pro data collection prior to 35 DAS resulted in limited to no plant structure reconstructed within the 3D point clouds, indicating that higher resolution imaging would be necessary to reconstruct early season plant structure. Out of 29 flights, 16 were observed to be of high quality, while only eight flight dates (35, 43, 57, 62, 65, 69, 100, and 117 DAS) conformed to statistical quality tests (File S1) and were used for the remainder of this study (Figure 1; Table S2).

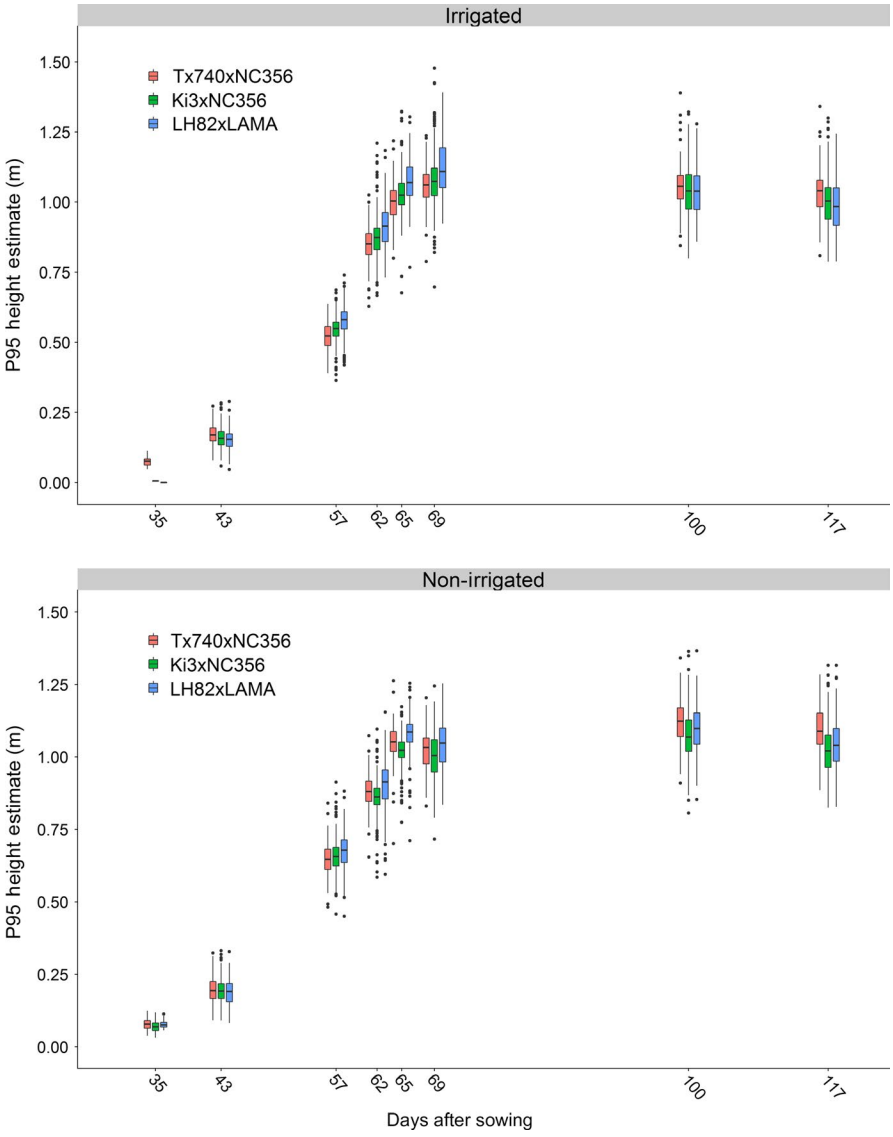

FIGURE 1 UAS P95 height estimates summarized by flight date. Although the three populations were genetically diverse, the mean growth patterns behaved similarly. Little differentiation could be seen early in the season between genotypes, where the measurement error may have been smaller that genotypic differences, as the plants reached their peak height and flowered, height differences became much greater

3.2 | Genetic variance decomposition

Variance component decomposition demonstrated total phenotypic variance increased throughout the growing season for all inbred populations (Figure 2, black circles), as has been found in hybrid trials (Pugh et al., 2018; Anderson, Murray, Malambo, et al., 2019). UAS phenotypic variance for height did not exceed manual, terminal plant height (PHT_{TRML}, Figure 2 M bar). Genetic variance averaged 51% (excluding 35 DAS) over the season fluctuating from flight to flight, but generally increasing until reaching a terminal height plateau. The proportion of variance attributed to genetics of plant height (PHT_{TRML}), as measured from the ground to the tip of the tassel, was numerically greater (irrigated: 62 ± 3%; non-irrigated: 52 ± 3), but not statistically (*t* test, $\alpha = 0.05$) different from genetic variance captured by UAS surveys. The ability of UAS P95 height estimates to capture equivalent genetic variation to manual measurements demonstrates the utility of UAS height estimates are a reliable, heritable phenotype alternative to manual height measurements in inbred maize populations.

3.3 | Sigmoidal modeling of UAS height estimates

Collection of comparable data sets through discrete timepoint UAS imagery becomes difficult when making comparisons across years, locations, and planting dates. Inconsistency in weather, quality of image collection, and relative maturity further reduces the probability of collecting comparable discrete timepoint UAS data sets. The collection of spatial–temporal flights combined with nonlinear curves provides comparable, heritable phenotypes (e.g., asymptote, inflection point, and growth rate) across environments, planting times, and genetic diversity (Anderson, Murray, Malambo, et al., 2019). The Weibull function was selected as the best fitting sigmoidal growth function for this data set compared with Logistic, Probit, and Gompertz functions based on the lowest information criteria value. The Weibull function model fits maize inbred temporal growth (mean $R^2 > 0.99$, RMSE ranging from 2.4 to 3.7 cm) across all populations and environment (Figure 3). Significant differences in asymptote, the maximum height, were only found between Tx740xNC356 (1.10 m) and LH82xLAMA (1.08 m) with a 2 cm difference in means under irrigation. LH82 (Holden's Foundation Seeds, 1985) is the earliest to flower and shortest of the inbred lines adaptable to these environments and had among the lowest asymptote and inflection point, but moderate growth rate.

In comparison, PHT_{TMRL} was significantly different across populations (1.66, 1.59, and 1.57 m) under irrigated conditions for Tx740xNC356, Ki3xNC356, and LH82xLAMA, respectively. The reduced means of the asymptote demonstrated the inherent biases of UAS estimation of plant height compared with manual measurements (Holman et al., 2016; Watanabe et al., 2017; Malambo et al., 2018;

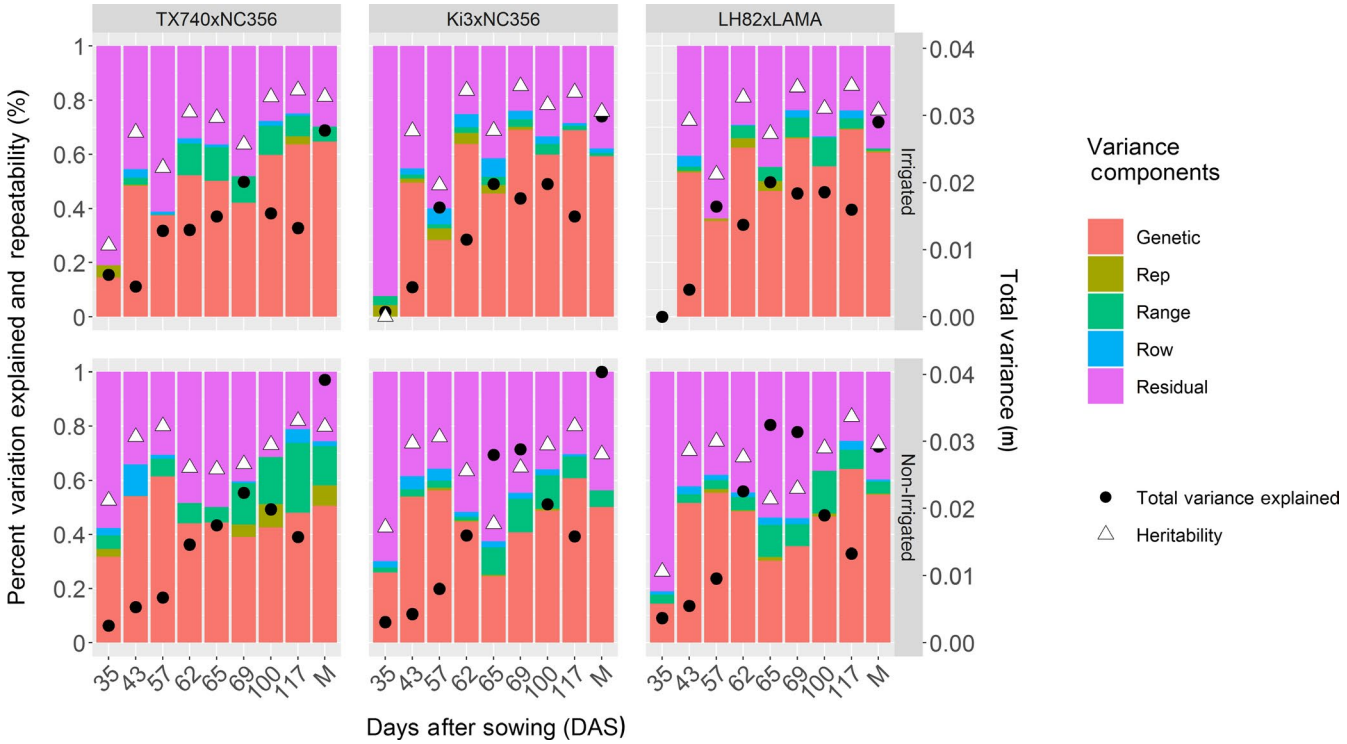

FIGURE 2 Variance component decomposition of UAS P95 height estimates. The percent variation explained in the model of equation (1) for individual UAS surveys of three RIL populations showed that genetic and residual (error) variation were the main drivers of variability observed. Total variance (black circles) increased as the plants grew over later flight dates and was higher for manual (M) than UAS measurements. That the percent variance measures and heritability were similar for M and UAS suggests that UAS compressed all variance sources similarly

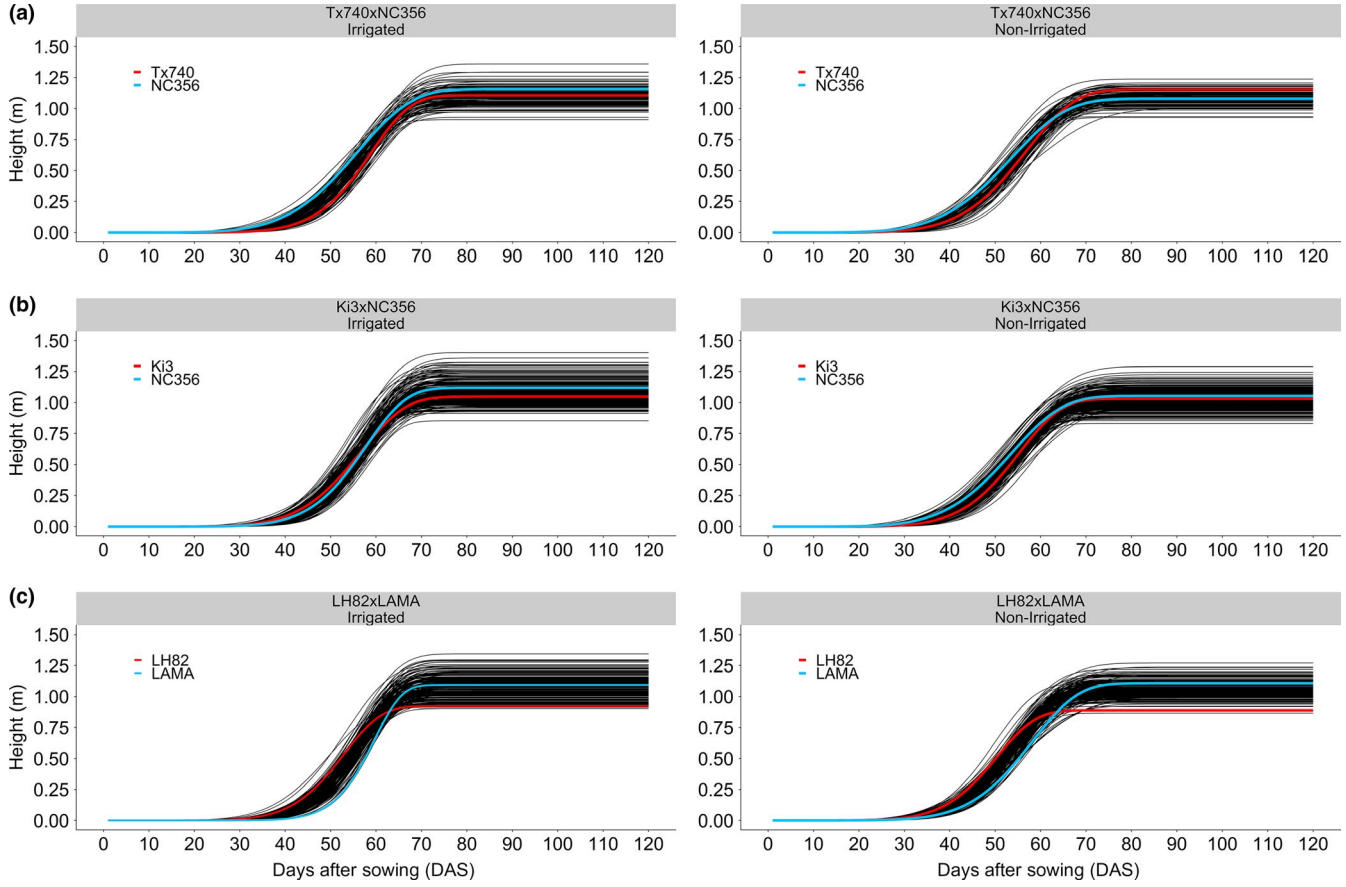

FIGURE 3 Nonlinear Weibull functional modeling of growth trajectories. Sigmoidal curves based off the Weibull function (equation (3)) effectively modeled the growth of each entry. For each population, the female parent (red line) and the male parent (blue line) crossed over demonstrating that early season height was not predictable by standard manual terminal height measurements

Anderson, Murray, Malambo, et al., 2019); ~0.5 m underestimate of height has been documented in past studies of hybrid maize at flight altitudes of 120 m (Anderson, Murray, Malambo, et al., 2019). The average difference in height estimates increased by ~5 and ~10 cm when compared to P99 and P100 point cloud estimates, indicating that the reduction was not caused solely by the lower percentile, P95. The combination of flight altitude and reduced plant canopy density of the inbreds likely biased the UAS toward shorter estimates. Biases aside, numerical rankings between asymptote and PHT_{TRML} were correctly consistent in ranking Tx740xNC356, Ki3xNC356, and LH82xLAMA population means from tallest to shortest and Pearson correlations (r) (irrigated: 0.77, 0.74, and 0.74; non-irrigated: 0.66, 0.72, and 0.74; Figures S1–S3) indicated highly significant (i.e., H_0: $r = 0$, $\alpha = 0.05$), positive linear correlations between UAS asymptotes estimates and PHT_{TRML} measurements.

The inflection point of the Weibull model is biologically important to identify the DAS in which maximum AGR is occurring; this point has been shown to be highly correlated with flowering time in hybrid trials (Anderson, Murray, Malambo, et al., 2019). Significant differences were found between each population's mean for inflection point (58.6, 58.0, and 57.5 d for Tx740xNC356, Ki3xNC356, and LH82xLAMA) within the irrigated trial (Figure 4c). Abiotic stress related to water limitations in non-irrigated trials delayed the inflection point by two days on average across the populations. Inflection point had low positive correlations to PHT_{TRML} (irrigated: 0.30, 0.27, and 0.34; non-irrigated: 0.02, 0.22, and 0.24; Figures S1–S3) but high correlations to flowering time (DTA/DTS) (irrigated: 0.60/0.45, 0.59/0.58, and 0.64/0.59; non-irrigated: 0.61/0.56, 0.55/0.53, and 0.68/0.66; Figures S1–S3). PHT P95 estimates were negatively correlated (r = −0.74: −0.50) with inflection points during the early season, but gradually progressed toward a positive correlation ~10 days after the mean inflection point (Figures S1–S3). Later inflection points had extended vegetative growth periods leading to taller plants, indicating the possibility of pleiotropic QTL for both flowering time and growth rate across the functional curve parameters. Because correlation was high but imperfect, tall genotypes with earlier inflection points could indicate better fitness in stressful environments, as these plants reach their terminal height quickly without regard to environmental stresses.

The Weibull growth rate parameter (b; empirical constant), influencing the steepness of the Weibull curve, significantly differed ($\alpha = 0.05$) in its means across the populations in both environments (irrigated: 6.9, 7.6, and 8.2; non-irrigated: 6.3, 6.5, and 6.8). The first derivative of the Weibull function (Equation 4), the absolute growth rate (AGR), calculated at the inflection point ($x = x_0$) equals

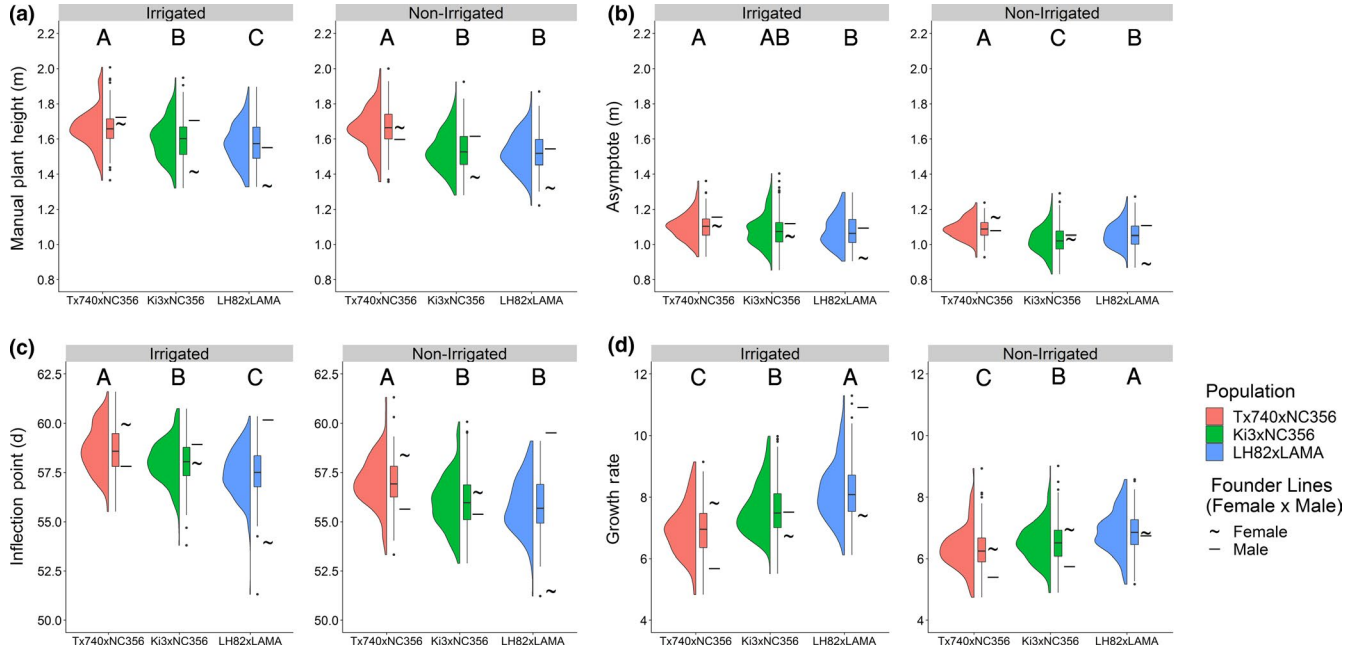

FIGURE 4 Distribution of Weibull functional parameters. Entry BLUPS of (a) manual terminal plant height, (b) Weibull asymptote, (c) Weibull inflection point, and (d) Weibull growth rate for each mapping population demonstrated variability both within and between these populations with substantial transgressive segregation in most cases. Letters above define significant differences in means at $\alpha = 0.05$

the maximum AGR. The maximum AGR occurred ~50–60 DAS, which was shortly before flowering, in this period cells are both dividing and elongating within the internodes above the ear node (Morrison, Kessler, & Buxton, 1994; Robertson, 1994; Fournier & Andrieu, 2000). Significant differences were found in the maximum AGR across populations within the irrigated trial (48, 52, and 56 mm/day), and LH82xLAMA was 3 mm/day greater than the other populations in the non-irrigated trial despite being the shortest population overall. A reduction in AGR was observed within the non-irrigated trial (4, 7, and 8 mm/day for Tx740xNC356, Ki3xNC356, and LH82xLAMA, respectively), compared to the irrigated trial, likely due to water stress during this period (Tardieu et al., 2005). Overall, this demonstrated that the AGR had heritable genetic diversity and was phenotypically plastic in response to different environmental conditions.

3.4 | QTL mapping

3.4.1 | Manual terminal height associations

Nine QTL were identified for PHTTRML across the three populations and two environments (Table S3) each explaining 5.1–9.4% of genetic variance. All PHTTRML associations had additive effects of ~3 cm (Table S3). One region was identified across two populations q1_172 (LH82xLAMA; irrigated) and q1_176 (Tx740xNC356; non-irrigated), localizing to the 280 to 284 Mbs region of chromosome 1. We identified a single genomic region, 98–128 Mbs on chromosome 2 that co-localized within the same genetic background (Ki3xNC356) across different environmental treatments (q2_70 irrigated and q2_69 non-irrigated). The limited co-localization of QTLs across bi-parental populations is part of the difficulty in identifying genomic regions that can be utilized in genetic backgrounds beyond those in which they were discovered (Beavis, 1998;Jannink, Bink, & Jansen, 2001). This also demonstrated the lack of statistical power in the smaller of the three populations Tx740xNC356 (n = 110). It has been empirically shown that population size is the most critical factor in QTL linkage mapping (Anderson et al., 2018).

3.4.2 | Functional parameter associations

Analysis of QTLsg using the three functional parameters of the Weibull curve as phenotypes identified 13, 9, and 12 significant marker associations with the asymptote, growth rate, and inflection point, respectively (Table S5). Asymptote QTLs explained genetic variation ranging from 3.4% to 14.3% with additive effects ranging from 2 to 5 cm, consistent with PHTTRML. High correlations between asymptote and PHTTRML indicated that similar QTL would likely be detected using both traits. Two PHTTRML QTLs, q1_172 LH82xLAMA (irrigated) and q1_176 Tx740xNC356 (non-irrigated), co-localized with an asymptote QTL, q1_173 of LH82xLAMA (irrigated) (Figure 5; Table S3). Additional co-localizations were found between q6_67 Tx740xNC356 (irrigated) asymptote and q6_62 Ki3xNC356 (irrigated) PHTTRML, as well as q8_10 LH82xLAMA (non-irrigated) asymptote with q8_14 Ki3xNC356 (irrigated) PHTTRML and q8_12 Ki3xNC356 (non-irrigated) PHTTRML. The limited co-localization and increased number of QTL associated with

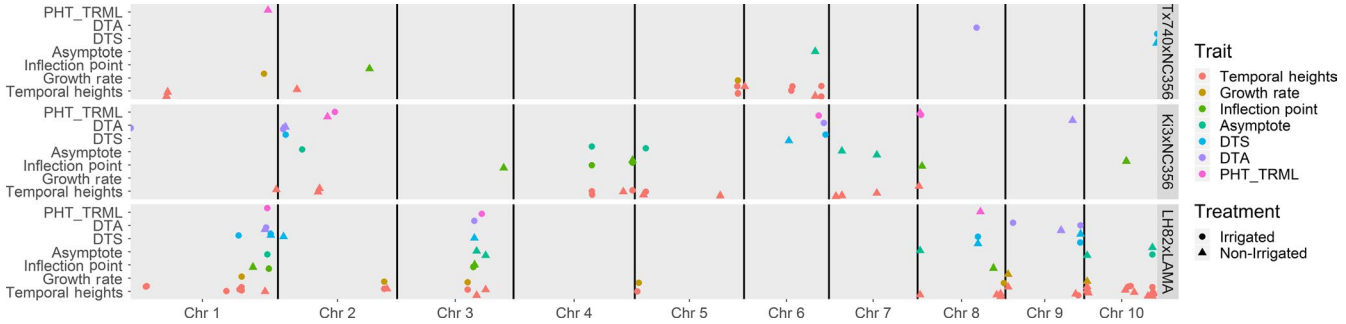

FIGURE 5 Co-localization of agronomic and functional growth QTL associations. Significant QTL co-localized across agronomic traits (PHT_TRML, manual, terminal plant height; DTA, days to anthesis; DTS, days to silking), functional growth parameters (asymptote, inflection point, growth rate), and temporal height estimates from the Weibull curves. Temporal expression of all height QTL can be visualized in Figure S4

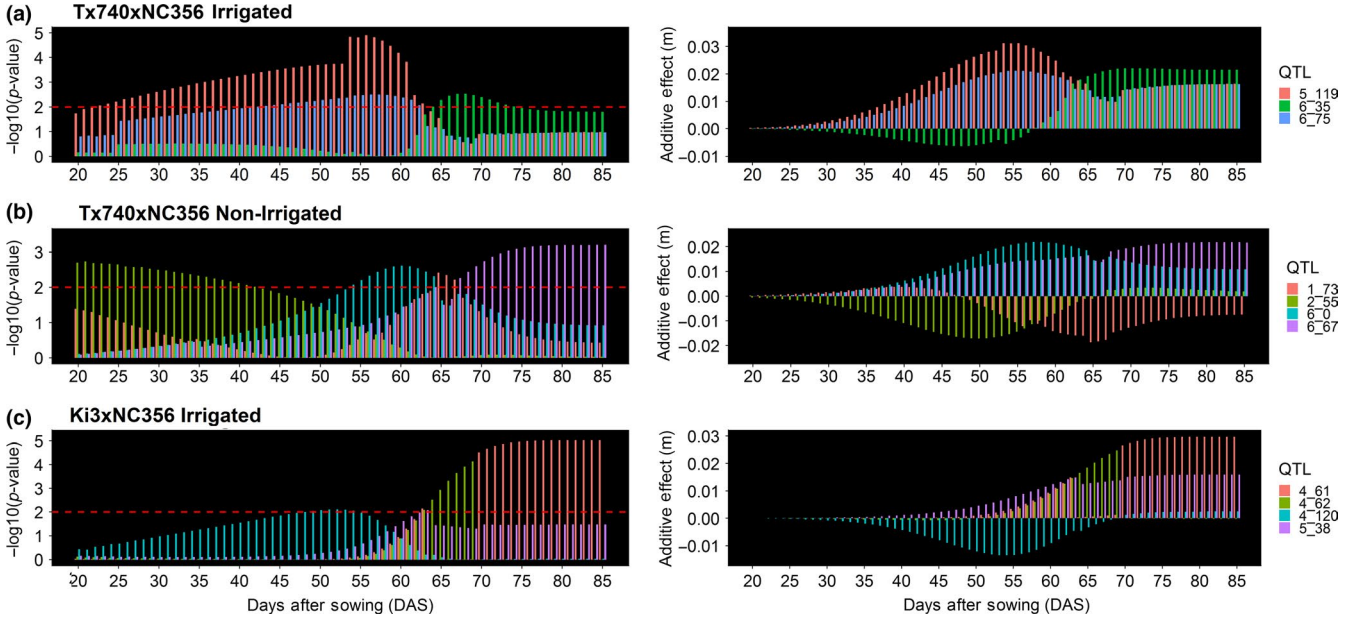

FIGURE 6 Visualization of temporal trends in QTL expression. Temporal trends in QTL expression were observed in all QTL across populations and environments. Most QTL were under the significance threshold (left side) of LOD = 2 (red dashed line) at some point during the growing season; however, the smaller additive effects (right side) during these periods would not have been expected to be declared a QTL

asymptote, compared to PHTTRML, demonstrate the application of a unique UAS phenotype to replace or work in conjunction with traditional phenotypes to identify genomic regions associated with complex, dynamic, quantitative traits such as maize plant height.

The seven growth rate QTL each explained 5.6 to 15% of the genotypic variance with additive effects ranging from 0.2 to 0.3 (Table S5). Inflection point QTL each explained 4.3–13% of the genotypic variance with additive effects ranging from 0.2 to 0.5 days (Table S5). Irrigated Ki3xNC356 trial *q*4_61 and irrigated LH82xLAMA *q*1_173/*q*1_176 were associated with inflection point and asymptote, while non-irrigated LH82xLAMA *q*10_20 was associated with inflection point and growth rate (Table S5). The co-localization of QTL associated with multiple parameters of the sigmoidal growth function indicated these regions more than others may have had an effect on defining the overall developmental trajectory of maize height. The limited number of co-localizations demonstrated these traits are both genetically variable and highly plastic with the environment.

Multiple QTL were identified within the LH82xLAMA trials for PHT_{TRML}, asymptote, inflection point, and flowering time (DTA/DTS; Table S4) within the 273 to 287 Mbs region of chromosome 1 and the 140 to 176 Mbs region of chromosome 3 (Figure 5). The QTL region of chromosome 3 harbors ZmMADS69 (GRMZM2G171650; Chr3: 158979321..159007265), a regulator of flowering time with pleiotropic effects on plant height. ZmMADS69 has higher expression levels in temperate compared to tropical germplasm, leading to significant detection in temperate by tropical crosses (Liang et al., 2019), such as LH82xLAMA among others (Hirsch et al., 2014;

Peiffer et al., 2014; Anderson et al., 2018). The identified region on chromosome 1 contained the viviparous8 (vp8; GRMZM2G010353; Chr1: 286390345..286398537) locus which exhibits dwarfism due to reduced cell proliferation (Lv et al., 2014). Both loci may be deterministic QTL (dQTL) because the differential allelic variation affected the whole growth process (Wu et al., 2004) and was unaffected by environmental stimuli; ZmMADS69 effect was not influenced by day length (Liang et al., 2019) and vp8 exhibited normal plant hormone response (Wu et al., 2004). These results coupled with basic biological understanding indicated that allelic changes in loci can have a fundamental impact on the functional growth trajectory of maize, in contrast to the small shift in phenotypic expression of a single trait. It is therefore understandable that these two "major genes" have been previously identified and described in multiple studies, while the smaller and ephemeral effect loci remain mostly unknown.

3.4.3 | Temporal QTL associations

In addition to detecting QTL for the three parameters of the Weibull function, 58 QTLs were also detected using individual daily heights from 20 to 85 DAS predicted using the Weibull function. Comparisons between the 20 to 85 DAS predicted heights identified between 4 and 20 unique QTLs, based on peak position, for each population by irrigation combination (Figure 5; Table S6). Comparison of mean physical distance of the flanking markers for each the 58 unique QTLs demonstrated 23 QTLs were within 1 Mbp of a plant height candidate gene and an additional 18 QTLs were less than 5 Mbp from a candidate gene. Most of the 58 unique QTLs demonstrated a very dynamic nature of QTL affecting plant height throughout the growing season. For example, q5_119 in the irrigated Tx740xNC356 trial was detected from 22 to 62 DAS explaining 21% of the genetic variation at 54 DAS (Figure 6a; Table S6). In comparison, q5_35 of irrigated Tx740xNC356 trial was detected from 66 to 74 DAS explaining 11% of the genetic variation at 67 DAS (Figure 6a). Temporal QTL association was different for each population across environmental treatments (i.e., irrigation) demonstrating differential genomic localization while maintaining similarities in temporal association. Specifically, within the Tx740xNC356 population, both irrigation regimens (i.e., environments) have a temporally broad QTL (q5_119 irrigated and q2_55 non-irrigated) prior to inflection point (~58 DAS), followed by QTLs detected at shorter temporal intervals after the inflection point and may relate to the elongation of specific internode groupings (Morrison et al., 1994; Robertson, 1994; Fournier & Andrieu, 2000). Additionally, trends in QTL temporal association between populations exhibited unique temporal association patterns. For example, Tx740xNC356 exhibited QTLs prior to the inflection point at early growth stages, whereas Ki3xNC356 exhibited no detectable QTLs until ~50 DAS. Low phenotypic variation could be the cause, as could greater numbers of smaller effect loci toward an infinitesimal model, which would be difficult to detect.

Identified QTLs demonstrated dynamic trends in additive phenotypic effects (Figure 6, right side). In general, these results showed that the additive effects found at the peak significance DAS of a temporal QTL are a result of the cumulative effect of a gradual increase in the effect size of each genomic region (Figure 6). QTLs with peak association early within the season had significantly smaller additive effect estimates than those at later points in the growing season; due to reduced overall variation across individuals in the population at early growth stages (e.g., Figure 6 q2_55). Some QTL effects (Figure 6b q6_0) also appeared to lose their association throughout season, likely due to their effects being statistically diluted by new QTL becoming significant (Figure 6b q6_67). While most individual QTL alleles maintained their directional effect (Figure 6a; q5_119 and *q*6_75), some surprisingly switched effect directions within the growing season (q6_35). Understanding the biological basis of this switching phenomena would be both interesting and important for optimizing plant growth. Caution should be used to interpret all of these QTL as loci that functionally affect height and plant growth rather than height QTL per se; loci affecting rooting, plant health, or photoperiod sensitivity all could impact measured plant height.

Analysis across the entire linkage map demonstrated that directional changes in additive effect size were present during the growing season (Table S4–S5). Within marker-assisted selection protocols, targeting consistent directional effects may result in greater gains than those of temporal bi-directional effects. Before additional work is conducted, temporal effect size should first be validated through near isogenic lines across genetic backgrounds or in heterogeneous inbred families (Tuinstra, Ejeta, & Goldsbrough, 1997). However, we speculate that the temporal trend of the effect size, like many QTL effects, remains dependent on the genetic background, abiotic, and biotic interactions experienced in each environment, as well as the G x E interactions. Assuming temporal shifts in directional effects are valid (e.g., not due to over inflations, false positives from limited population size) then statistical models accounting for directional effect shifts will be necessary to incorporate temporal data sets of dynamic, quantitative traits within prediction modeling approaches for plant breeding, such as genomic selection.

4 | CONCLUSIONS

This study demonstrated that UAS height estimates of RIL mapping populations are highly heritable. Significant differences among the functional parameter phenotypes identified 32 functional QTL compared to the nine QTL identified by PHT_{TRML} measurements. Limited co-localization between functional, temporal, and PHT_{TRML} QTL demonstrated novel genetic loci effect the overall growth trajectory of maize, and that many of these QTL cannot be detected by conventional terminal measurements alone. Temporal mapping of height estimates demonstrated unique and dynamic patterns in QTL expression and effect sizes across different genetic background and environments. Finally, this work demonstrated that the additive effect of a QTL is cumulative resulting in a gradual increase in effect size of each genomic region. Efficient integration of temporal phenotyping via HTPP, such as UAS, will improve the scientific

understanding of dynamic, quantitative traits and developmental trajectories of important agronomic crops, leading to new understanding of plant biology. We present one of the first applications of UAS phenotyping of temporal growth across the growing season using UAS imagery on several genetic mapping populations. Here, we presented, for the first time, the dynamic nature of quantitative trait loci over time under field conditions. To our knowledge, this is first empirical study to expand beyond selective developmental time points (Wang et al., 2019), evaluating functional and temporal QTL expression in maize throughout the growing season within a field-based environment.

ACKNOWLEDGMENTS

The authors would like to acknowledge Misty Miles for coordinating the flight teams and providing administrative support, David Rooney, Jacob Pekar, and Stephen Labar for their agronomic and technical support, and graduate students and undergraduate/high school employees of the Texas A&M Quantitative Genetics and Maize Breeding program for their hard work and effort maintaining fields and collecting phenotypic data. All members of the Texas A&M UAS project for their collaboration without implementation UAS at Texas A&M would not have been so successful.

CONFLICTS OF INTEREST

The authors declare no conflict of interest associated with the work described in this manuscript.

AUTHOR CONTRIBUTION

S.L.A. conceptualized the study, curated the data, performed formal analysis, involved in investigation, contributed to methodology, wrote the original draft of the manuscript, reviewed and edited the manuscript, supervised the study, performed validation process, and visualized the data. S.C.M. conceptualized the study, acquired the funding, contributed to methodology, involved in project administration, supervised the study, provided resources, and reviewed and edited the manuscript. Y.C. curated the data, contributed to methodology, and reviewed and edited the manuscript. L.M. curated the data, performed formal analysis, involved in investigation, contributed to methodology, reviewed and edited the manuscript, and helped with software. S.P. conceptualized the study, acquired the funding, provided resources, reviewed and edited the manuscript, helped with software, and supervised the study. D.C. conceptualized the study, acquired the funding, provided resources, reviewed and edited the manuscript, and supervised the study. A.C. conceptualized the study, curated the data, performed formal analysis, involved in investigation, contributed to methodology, reviewed and edited the manuscript, and helped with software. J.J. conceptualized the study, curated the data, performed formal analysis, involved in investigation, contributed to methodology, provided resources, reviewed and edited the manuscript, helped with software, and supervised the study. S.C.M. agrees to serve as the author responsible for contact and ensures communication.

DATA AVAILABILITY STATEMENT

All the raw and processed data relevant to this study are publicly available on Dryad Digital Repository (Anderson, Murray, Chen, et al., 2019). All raw and processed image output files from this study are publicly available and can be obtained by request to the authors.

REFERENCES

AgiSoft PhotoScan Professional (2016) (Version 1.2.6) (Software). Retrieved from http://www.agisoft.com/downloads/installer/

Anderson, S., Murray, S., Chen, Y., Malambo, L., Chang, A., Popescu, S., … Jung, J. (2019). Unoccupied aerial system enabled functional modeling of maize (*Zea mays* L.) height reveals dynamic expression of loci associated to temporal growth, v6. Dryad, Dataset. https://doi.org/10.5061/dryad.q573n5tf2

Anderson, S. L., Mahan, A. L., Murray, S. C., & Klein, P. E. (2018). Four parent maize (FPM) population: Effects of mating designs on linkage disequilibrium and mapping quantitative traits. *The Plant Genome*, *11*.

Anderson, S. L., Murray, S., Malambo, L., Ratcliff, C., Popescu, S., Cope, D., … Thomasson, J. A. (2019). Prediction of maize grain yield before maturity using improved temporal height estimates of unmanned aerial systems. *The Plant Phenome Journal*, *2*.

Anthony, D., Elbaum, S., Lorenz, A., & Detweiler, C. (2014) On crop height estimation with UAVs. In Intelligent Robots and Systems (IROS 2014), 2014 IEEE/RSJ International Conference on. IEEE, pp. 4805–4812.

Araus, J. L., & Cairns, J. E. (2014). Field high-throughput phenotyping: The new crop breeding frontier. *Trends in Plant Science*, *19*, 52–61.

Araus, J. L., Kefauver, S. C., Zaman-Allah, M., Olsen, M. S., & Cairns, J. E. (2018). Translating high-throughput phenotyping into genetic gain. *Trends in Plant Science*, *23*(5), 451–466.

Archontoulis, S. V., & Miguez, F. E. (2015). Nonlinear regression models and applications in agricultural research. *Agronomy Journal*, *107*, 786–798.

Bac-Molenaar, J. A., Vreugdenhil, D., Granier, C., & Keurentjes, J. J. (2015). Genome-wide association mapping of growth dynamics detects time-specific and general quantitative trait loci. *Journal of Experimental Botany*, *66*, 5567–5580.

Beavis, W. D. (1998). QTL analyses: Power, precision, and accuracy. *Molecular Dissection of Complex Traits*, *1998*, 145–162.

Bendig, J., Bolten, A., Bennertz, S., Broscheit, J., Eichfuss, S., & Bareth, G. (2014). Estimating biomass of barley using crop surface models (CSMs) derived from UAV-based RGB imaging. *Remote Sensing*, *6*, 10395–10412.

Campbell, M. T., Du, Q., Liu, K., Brien, C. J., Berger, B., Zhang, C., & Walia, H. (2017). A comprehensive image-based phenomic analysis reveals the complex genetic architecture of shoot growth dynamics in rice (*Oryza sativa*). *The Plant Genome*, *10*.

Chang, A., Jung, J., Maeda, M. M., & Landivar, J. (2017). Crop height monitoring with digital imagery from unmanned aerial system (UAS). *Computers and Electronics in Agriculture*, *141*, 232–237.

Chen, D.-H., & Ronald, P. (1999). A rapid DNA minipreparation method suitable for AFLP and other PCR applications. *Plant Molecular Biology Reporter*, *17*, 53–57.

Chen, Y. (2016). High-density linkage map construction, mapping of agronomic traits in tropical maize (*Zea mays* L.) and validating SNPs controlling maize grain yield and plant height in southern hybrid testcrosses. Doctoral dissertation. Texas A&M University. Available from http://hdl.handle.net/1969.1/158620.

Chu, T., Starek, M. J., Brewer, M. J., Murray, S. C., & Pruter, L. S. (2018). Characterizing canopy height with UAS structure-from-motion photogrammetry—results analysis of a maize field trial with respect to multiple factors. *Remote Sensing Letters*, *9*, 753–762.

De Souza, C. H. W., Lamparelli, R. A. C., Rocha, J. V., & Magalhães, P. S. G. (2017). Height estimation of sugarcane using an unmanned aerial

system (UAS) based on structure from motion (SfM) point clouds. *International Journal of Remote Sensing*, *38*, 2218–2230.

Farfan, I. D. B., Gerald, N., Murray, S. C., Isakeit, T., Huang, P.-C., Warburton, M., … Kolomiets, M. (2015). Genome wide association study for drought, aflatoxin resistance, and important agronomic traits of maize hybrids in the sub-tropics. *PLoS ONE*, *10*, e0117737.

Farfan, I. D. B., Murray, S. C., Labar, S., & Pietsch, D. (2013). A multi-environment trial analysis shows slight grain yield improvement in Texas commercial maize. *Field Crops Research*, *149*, 167–176.

Feldman, M. J., Paul, R. E., Banan, D., Barrett, J. F., Sebastian, J., Yee, M.-C., … Dinneny, J. R. (2017). Time dependent genetic analysis links field and controlled environment phenotypes in the model C4 grass Setaria. *PLoS Genetics*, *13*, e1006841.

Ferreira, F. J., & Kieber, J. J. (2005). Cytokinin signaling. *Current Opinion in Plant Biology*, *8*, 518–525.

Finkelstein, R. R. (2006). Studies of abscisic acid perception finally flower. *The Plant Cell*, *18*, 786–791.

Fournier, C., & Andrieu, B. (2000). Dynamics of the elongation of internodes in maize (*Zea mays* L.): Analysis of phases of elongation and their relationships to phytomer development. *Annals of Botany*, *86*, 551–563.

Furbank, R. T., & Tester, M. (2011). Phenomics–technologies to relieve the phenotyping bottleneck. *Trends in Plant Science*, *16*, 635–644.

Geipel, J., Link, J., & Claupein, W. (2014). Combined spectral and spatial modeling of corn yield based on aerial images and crop surface models acquired with an unmanned aircraft system. *Remote Sensing*, *6*, 10335–10355.

Gonda, I., Ashrafi, H., Lyon, D. A., Strickler, S. R., Hulse-Kemp, A. M., Ma, Q., … Futrell, S. (2018). Sequencing-based bin map construction of a tomato mapping population, facilitating high-resolution quantitative trait loci detection. *The Plant Genome*, *12*.

Han, L., Yang, G., Dai, H., Xu, B., Yang, H., Feng, H., … Yang, X. (2019). Modeling maize above-ground biomass based on machine learning approaches using UAV remote-sensing data. *Plant Methods*, *15*, 10.

Han, L., Yang, G., Yang, H., Xu, B., Li, Z., & Yang, X. (2018). Clustering field-based maize phenotyping of plant-height growth and canopy spectral dynamics using a UAV remote-sensing approach. *Frontiers in Plant Science*, *9*, 1638.

Hartwig, T., Chuck, G. S., Fujioka, S., Klempien, A., Weizbauer, R., Potluri, D. P. V., … Schulz, B. (2011). Brassinosteroid control of sex determination in maize. *Proceedings of the National Academy of Sciences*, *108*, 19814–19819.

Hirsch, C. N., Foerster, J. M., Johnson, J. M., Sekhon, R. S., Muttoni, G., Vaillancourt, B., … Barry, K. (2014). Insights into the maize pan-genome and pan-transcriptome. *The Plant Cell*, *26*, 121–135.

Holden's Foundation Seeds I (1985) *Corn 'LH82'*. PVP Office.

Holman, F. H., Riche, A. B., Michalski, A., Castle, M., Wooster, M. J., & Hawkesford, M. J. (2016). High throughput field phenotyping of wheat plant height and growth rate in field plot trials using UAV based remote sensing. *Remote Sensing*, *8*, 1031.

Huq, E. (2006). Degradation of negative regulators: A common theme in hormone and light signaling networks? *Trends in Plant Science*, *11*, 4–7.

Jannink, J.-L., Bink, M. C., & Jansen, R. C. (2001). Using complex plant pedigrees to map valuable genes. *Trends in Plant Science*, *6*, 337–342.

JMP® (2018) Version 14.0.0. SAS Institute Inc., Cary, NC, 1989–2018.

Katsvairo, T. W., Cox, W. J., & Van Es, H. M. (2003). Spatial growth and nitrogen uptake variability of corn at two nitrogen levels. *Agronomy Journal*, *95*, 1000–1011.

Lawit, S. J., Wych, H. M., Xu, D., Kundu, S., & Tomes, D. T. (2010). Maize DELLA proteins dwarf plant8 and dwarf plant9 as modulators of plant development. *Plant and Cell Physiology*, *51*, 1854–1868.

Li, H., Ye, G., & Wang, J. (2007). A modified algorithm for the improvement of composite interval mapping. *Genetics*, *175*, 361–374.

Li, W., Niu, Z., Chen, H., Li, D., Wu, M., & Zhao, W. (2016). Remote estimation of canopy height and aboveground biomass of maize using high-resolution stereo images from a low-cost unmanned aerial vehicle system. *Ecological Indicators*, *67*, 637–648.

Liang, Y., Liu, Q., Wang, X., Huang, C., Xu, G., Hey, S., … Wu, L. (2019). Zm MADS 69 functions as a flowering activator through the ZmRap2. 7-ZCN 8 regulatory module and contributes to maize flowering time adaptation. *New Phytologist*, *221*, 2335–2347.

Lorenzo, O., & Solano, R. (2005). Molecular players regulating the jasmonate signalling network. *Current Opinion in Plant Biology*, *8*, 532–540.

Lv, H., Zheng, J., Wang, T., Fu, J., Huai, J., Min, H., … Wang, G. (2014). The maize d2003, a novel allele of VP8, is required for maize internode elongation. *Plant Molecular Biology*, *84*, 243–257.

Lyra, D. H., Virlet, N., Sadeghi-Tehran, P., Hassall, K. L., Wingen, L. U., Orford, S., … Slavov, G. T. (2020). Functional QTL mapping and genomic prediction of canopy height in wheat measured using a robotic field phenotyping platform. *Journal of Experimental Botany*, *71*, 1885–1898.

Machado, S., Bynum, E., Archer, T., Lascano, R., Wilson, L., Bordovsky, J., … Xu, W. (2002). Spatial and temporal variability of corn growth and grain yield. *Crop Science*, *42*, 1564–1576.

Mahan, A. L., Murray, S. C., & Klein, P. E. (2018). Four-parent maize (FPM) population: development and phenotypic characterization. *Crop Science*, *58*, 1106–1117.

Makarevitch, I., Thompson, A., Muehlbauer, G. J., & Springer, N. M. (2012). Brd1 gene in maize encodes a brassinosteroid C-6 oxidase. *PLoS ONE*, *7*, e30798.

Malambo, L., Popescu, S., Murray, S., Putman, E., Pugh, N., Horne, D., … Avant, R. (2018). Multitemporal field-based plant height estimation using 3D point clouds generated from small unmanned aerial systems high-resolution imagery. *International Journal of Applied Earth Observation and Geoinformation*, *64*, 31–42.

Mallarino, A., Oyarzabal, E., & Hinz, P. (1999). Interpreting within-field relationships between crop yields and soil and plant variables using factor analysis. *Precision Agriculture*, *1*, 15–25.

Mayfield, K., Betrán, F. J., Isakeit, T., Odvody, G., Murray, S. C., Rooney, W. L., & Landivar, J. C. (2012). Registration of maize germplasm lines Tx736, Tx739, and Tx740 for reducing preharvest aflatoxin accumulation. *Journal of Plant Registrations*, *6*, 88–94.

Morrison, T., Kessler, J., & Buxton, D. (1994). Maize internode elongation patterns. *Crop Science*, *34*, 1055–1060.

Multani, D. S., Briggs, S. P., Chamberlin, M. A., Blakeslee, J. J., Murphy, A. S., & Johal, G. S. (2003). Loss of an MDR transporter in compact stalks of maize br2 and sorghum dw3 mutants. *Science*, *302*, 81–84.

Muraya, M. M., Chu, J., Zhao, Y., Junker, A., Klukas, C., Reif, J. C., & Altmann, T. (2017). Genetic variation of growth dynamics in maize (*Zea mays* L.) revealed through automated non-invasive phenotyping. *The Plant Journal*, *89*, 366–380.

Neumann, K., Zhao, Y., Chu, J., Keilwagen, J., Reif, J. C., Kilian, B., & Graner, A. (2017). Genetic architecture and temporal patterns of biomass accumulation in spring barley revealed by image analysis. *BMC Plant Biology*, *17*, 137.

Pauli, D., Andrade-Sanchez, P., Carmo-Silva, A. E., Gazave, E., French, A. N., Heun, J., … Strand, R. J. (2016). Field-based high-throughput plant phenotyping reveals the temporal patterns of quantitative trait loci associated with stress-responsive traits in cotton. *G3: Genes|Genomes|Genetics*, *6*, 865–879.

Pauli, D., Chapman, S. C., Bart, R., Topp, C. N., Lawrence-Dill, C. J., Poland, J., & Gore, M. A. (2016). The quest for understanding phenotypic variation via integrated approaches in the field environment. *Plant Physiology*, *172*, 622–634.

Peiffer, J. A., Romay, M. C., Gore, M. A., Flint-Garcia, S. A., Zhang, Z., Millard, M. J., … Bradbury, P. J. (2014). The genetic architecture of maize height. *Genetics*, *196*, 1337–1356.

Pix4Dmapper (2018). Pix4D SA. www.pix4d.com

Pugh, N., Horne, D. W., Murray, S. C., Carvalho, G., Malambo, L., Jung, J., … Chu, T. (2018). Temporal estimates of crop growth in sorghum

and maize breeding enabled by unmanned aerial systems. *The Plant Phenome Journal*, *1*.

Robertson, M. (1994). Relationships between internode elongation, plant height and leaf appearance in maize. *Field Crops Research*, *38*, 135–145.

Sankaran, S., Khot, L. R., Espinoza, C. Z., Jarolmasjed, S., Sathuvalli, V. R., Vandemark, G. J., … Knowles, N. R. (2015). Low-altitude, high-resolution aerial imaging systems for row and field crop phenotyping: A review. *European Journal of Agronomy*, *70*, 112–123.

Shi, Y., Thomasson, J. A., Murray, S. C., Pugh, N. A., Rooney, W. L., Shafian, S., … Neely, H. L. (2016). Unmanned aerial vehicles for high-throughput phenotyping and agronomic research. *PLoS ONE*, *11*, e0159781.

Tanger, P., Klassen, S., Mojica, J. P., Lovell, J. T., Moyers, B. T., Baraoidan, M., … Bush, D. R. (2017). Field-based high throughput phenotyping rapidly identifies genomic regions controlling yield components in rice. *Scientific Reports*, *7*, 42839.

Tardieu, F., Reymond, M., Muller, B., Granier, C., Simonneau, T., Sadok, W., & Welcker, C. (2005). Linking physiological and genetic analyses of the control of leaf growth under changing environmental conditions. *Australian Journal of Agricultural Research*, *56*, 937–946.

Tuinstra, M., Ejeta, G., & Goldsbrough, P. (1997). Heterogeneous inbred family (HIF) analysis: A method for developing near-isogenic lines that differ at quantitative trait loci. *Theoretical and Applied Genetics*, *95*, 1005–1011.

Varela, S., Assefa, Y., Prasad, P. V., Peralta, N. R., Griffin, T. W., Sharda, A., … Ciampitti, I. A. (2017). Spatio-temporal evaluation of plant height in corn via unmanned aerial systems. *Journal of Applied Remote Sensing*, *11*, 036013.

Wallace, J. G., Zhang, X., Beyene, Y., Semagn, K., Olsen, M., Prasanna, B. M., & Buckler, E. S. (2016). Genome-wide association for plant height and flowering time across 15 tropical maize populations under managed drought stress and well-watered conditions in Sub-Saharan Africa. *Crop Science*, *56*, 2365–2378.

Wang, X., Zhang, R., Song, W., Han, L., Liu, X., Sun, X., … Yang, H. (2019). Dynamic plant height QTL revealed in maize through remote sensing phenotyping using a high-throughput unmanned aerial vehicle (UAV). *Scientific Reports*, *9*, 3458.

Wang, Y., Zhao, J., Lu, W., & Deng, D. (2017). Gibberellin in plant height control: Old player, new story. *Plant Cell Reports*, *36*, 1–8.

Ward, B., Brien, C., Oakey, H., Pearson, A., Negrão, S., Schilling, R. K., … Roy, S. J. (2019). High-throughput 3D modelling to dissect the genetic control of leaf elongation in barley (*Hordeum vulgare*). *Plant Journal*, *98*, 555–570.

Watanabe, K., Guo, W., Arai, K., Takanashi, H., Kajiya-Kanegae, H., Kobayashi, M., … Tsutsumi, N. (2017). High-throughput phenotyping of sorghum plant height using an unmanned aerial vehicle and its application to genomic prediction modeling. Frontiers. *Plant Science*, *8*.

Winkler, R. G., & Helentjaris, T. (1995). The maize Dwarf3 gene encodes a cytochrome P450-mediated early step in Gibberellin biosynthesis. *Plant Cell*, *7*, 1307–1317.

Wu, R., & Lin, M. (2006). Functional mapping—how to map and study the genetic architecture of dynamic complex traits. *Nature Reviews Genetics*, *7*, 229–237.

Wu, R., Wang, Z., Zhao, W., & Cheverud, J. M. (2004). A mechanistic model for genetic machinery of ontogenetic growth. *Genetics*, *168*, 2383–2394.

Würschum, T., Liu, W., Busemeyer, L., Tucker, M. R., Reif, J. C., Weissmann, E. A., … Maurer, H. P. (2014). Mapping dynamic QTL for plant height in triticale. *BMC Genetics*, *15*, 59.

Xavier, A., Hall, B., Hearst, A. A., Cherkauer, K. A., & Rainey, K. M. (2017). Genetic architecture of phenomic-enabled canopy coverage in glycine max. *Genetics*, *206*, 1081–1089.

Yin, X., McClure, M. A., Jaja, N., Tyler, D. D., & Hayes, R. M. (2011). In-season prediction of corn yield using plant height under major production systems. *Agronomy Journal*, *103*, 923–929.

Zhang, X., Huang, C., Wu, D., Qiao, F., Li, W., Duan, L., … Liu, Q. (2017). High-throughput phenotyping and QTL mapping reveals the genetic architecture of maize plant growth. *Plant Physiology*, *173*, 1554–1564.

SUPPORTING INFORMATION

Additional supporting information may be found online in the Supporting Information section.

How to cite this article: Anderson SL II, Murray SC, Chen Y, et al. Unoccupied aerial system enabled functional modeling of maize height reveals dynamic expression of loci. *Plant Direct*. 2020;4:1–13. https://doi.org/10.1002/pld3.223